AGU PUBLICATIONS

Global Biogeochemical Cycles

RESEARCH ARTICLE
10.1002/2017GB005744

Key Points:
- A chlorophyll fluorescence scheme is implemented in a land surface model
- The wilting point is the key parameter linking the carbon and water cycles
- Satellite observations lead to advances in understanding carbon-water cycles

Supporting Information:
- Supporting Information S1
- Table S1
- Figure S1

Correspondence to:
Y. Xue,
yxue@geog.ucla.edu

Citation:
Qiu, B., Xue, Y., Fisher, J. B., Guo, W., Berry, J. A., & Zhang, Y. (2018). Satellite chlorophyll fluorescence and soil moisture observations lead to advances in the predictive understanding of global terrestrial coupled carbon-water cycles. *Global Biogeochemical Cycles*, *32*. https://doi.org/10.1002/2017GB005744

Received 19 JUN 2017
Accepted 16 FEB 2018
Accepted article online 20 FEB 2018

Satellite Chlorophyll Fluorescence and Soil Moisture Observations Lead to Advances in the Predictive Understanding of Global Terrestrial Coupled Carbon-Water Cycles

Bo Qiu[1,2,3], Yongkang Xue[2], Joshua B. Fisher[4], Weidong Guo[1,5], Joseph A. Berry[6], and Yongguang Zhang[3]

[1]CMA-NJU Joint Laboratory for Climate Prediction Studies, Institute for Climate and Global Change Research, School of Atmospheric Sciences, Nanjing University, Nanjing, China, [2]Department of Geography and Department of Atmospheric and Oceanic Sciences, University of California, Los Angeles, CA, USA, [3]Jiangsu Provincial Key Laboratory of Geographic Information Science and Technology, International Institute for Earth System Sciences, Nanjing University, Nanjing, China, [4]Jet Propulsion Laboratory, California Institute of Technology, Pasadena, CA, USA, [5]Joint International Research Laboratory of Atmospheric and Earth System Sciences, Nanjing, China, [6]Department of Global Ecology, Carnegie Institution of Washington, Stanford, CA, USA

Abstract The terrestrial carbon and water cycles are coupled through a multitude of connected processes among soil, roots, leaves, and the atmosphere. The strength and sensitivity of these couplings are not yet well known at the global scale, which contributes to uncertainty in predicting the terrestrial water and carbon budgets. We now have synchronous, global-scale satellite observations of critical terrestrial carbon and water cycle components: solar-induced chlorophyll fluorescence (SIF) and soil moisture. We used these observations within the framework of a global terrestrial biosphere model (Simplified Simple Biosphere Model version 2.0, SSiB2) to investigate carbon-water coupling processes. We updated SSiB2 to include a mechanistic representation of SIF and tested the sensitivity of model parameters to improve the simulation of both SIF and soil moisture with the ultimate objective of improving the first-order terrestrial carbon component, gross primary production. Although several vegetation parameters, such as leaf area index and the green leaf fraction, improved the simulated SIF, and several soil parameters, such as hydraulic conductivity, improved simulated soil moisture, their effects were mainly limited to their respective cycles. One root-mean-square error parameter emerged as the key coupler between the carbon and water cycles: the wilting point. Updates to the wilting point significantly improved the simulations for SIF and gross primary production although substantial mismatches with the satellite data still existed. This study demonstrates the value of synchronous global measurements of the terrestrial carbon and water cycles in improving the understanding of coupled carbon-water cycles.

1. Introduction

Plant photosynthesis is an important process in the land surface model. There is substantial uncertainty in the simulation of the carbon cycle (Bonan et al., 2011; Friedlingstein et al., 2006; Wang et al., 2011) despite considerable progress in developments of observational data sets and models. This problem is rooted in the proper measurements of photosynthesis across scales (Fisher et al., 2014). Droughts potentially reduce the ability of the terrestrial biosphere to mitigate rising atmospheric CO_2 levels through primary production. For example, traditional greenness-based vegetation indices have been used for the estimation of the photosynthesis products. This approach for estimating potential photosynthesis from greenness indices provides a good understanding of the global biosphere (Running et al., 2004; Turner et al., 2003). However, these traditional greenness indices provide estimates of potential photosynthesis and cannot describe actual processes of photosynthesis and downregulation when plants experience environmental stresses (Meroni et al., 2008). Thus, a new approach to the direct estimation of photosynthesis through space-based proxies is desired for monitoring and modeling of carbon cycling.

Recent advancement in the remote sensing of solar-induced chlorophyll fluorescence (SIF) provides a novel way to directly estimate actual photosynthesis from space (Frankenberg, Butz, et al., 2011; Frankenberg, O'Dell, et al., 2011; Guanter et al., 2007; Joiner et al., 2011). Approximately 1–2% of the solar energy absorbed by chlorophyll is re-emitted as fluorescence. This fluorescence is essentially a "glow" of plants at wavelengths between 650 and about 800 nm. The fluorescence has two peak emissions at 685 and 740 nm, which are specific for plants (Lichtenthaler & Rinderle, 1988). The absorbed photosynthetically active radiation by a leaf can be used to drive photochemical reactions to reduce atmospheric CO_2, be re-emitted as fluorescence at longer wavelengths, or be lost through regulated nonphotochemical quenching processes (Baker, 2008). When plants experience environmental stresses and nonphotochemical quenching increases, both photosynthesis and fluorescence generally decrease.

Global retrieval of chlorophyll fluorescence has opened up a new approach to establishing a direct link between remotely sensed SIF and terrestrial photosynthetic processes. For example, previous studies (Frankenberg, O'Dell, et al., 2011; Guanter et al., 2014) have shown that SIF products from the Japan Aerospace Exploration Agency Greenhouse gases Observing SATellite (GOSAT) and the Global Ozone Monitoring Experiment-2 (GOME-2) satellite are linearly correlated with terrestrial photosynthesis or gross primary production (GPP). Using the near-surface measurement of canopy-scale SIF data at 760 nm in temperate deciduous forests, Yang et al. (2015) found that SIF correlated with GPP at diurnal and seasonal scales. The study conducted by Guanter et al. (2014) showed that satellite SIF measurements are more sensitive to the high photosynthetic rates of cropland than are other remotely sensed vegetation parameters, and SIF does not have the same linearity with GPP for different ecosystems, which makes the proper mechanistic representation of SIF to GPP highly important and necessary. Furthermore, Lee et al. (2013) showed that GOSAT SIF products have clear water stress signals over tropical rain forests. The normalized difference vegetation index or other similar indices, however, does not capture the signals well. Moreover, using the Orbiting Carbon Observatory-2 (OCO-2) satellite data, Sun et al. (2017) found that the SIF-GPP relationships at eddy covariance flux sites in the vicinity of OCO-2 orbital tracks were more consistent across biomes than previously suggested.

Water and carbon cycles are closely coupled by plant biochemical processes through photosynthesis (Scholze et al., 2016). The physiological effects of droughts lead to a decrease in the light use efficiency for photosynthesis on the leaf scale. It has been shown that drought also causes a decrease in fluorescence yield (Flexas et al., 2002). Sun et al. (2015) used GOME-2 satellite data to explore the potential of SIF for monitoring drought dynamics, and the results showed that negative SIF anomalies in the spatial patterns are very similar to the drought intensity maps from the U.S. Drought Monitor for droughts of 2011 in Texas and 2012 over the central Great Plains. After examining satellite-based measurements of SIF over the region impacted by the Russian drought and heat wave of 2010, Yoshida et al. (2015) found that SIF measurements were sensitive to the fraction of absorbed photosynthetically active radiation.

Droughts and associated heat waves have a direct impact on plant photosynthesis through the physiological response to water deficit and high temperature, including reductions in enzyme activity and stomatal conductance to prevent water loss. The plant photosynthesis responses to drought differ among vegetation types because stomatal conductance differs among ecosystems (Blackman et al., 2009). Moreover, canopy light use efficiency, which is often used to estimate GPP in remote sensing, is closely related to soil moisture and certain other environmental factors in satellite measurements (Madani et al., 2014). Scholze et al. (2016) found that the assimilation of satellite soil moisture data could improve the estimation of atmospheric CO_2 in the Carbon Cycle Data Assimilation System.

This paper integrates soil moisture data from the Soil Moisture and Ocean Salinity (SMOS) mission conducted by the European Space Agency (Kerr et al., 2010) and fluorescence measurements from GOSAT (Frankenberg, Butz, et al., 2011; Frankenberg, O'Dell, et al., 2011) to evaluate the global impacts of these products on estimations of carbon budgets and to investigate broad-scale relationships between soil moisture and SIF. We coupled a chlorophyll fluorescence model (Lee et al., 2015; van der Tol et al., 2014) into a well-established global terrestrial biosphere model (Simplified Simple Biosphere Model version 2.0, SSiB2) (Qiu et al., 2016; Xue et al., 1991; Xue, Fennessy, et al., 1996; Zhan et al., 2003). The SIF data were used to evaluate the simulation of photosynthesis as a diagnostic tool. To understand process-level mechanistic processes, we integrated two satellite measurements into SSiB2 to improve the model parameterization as well as to evaluate the model-simulated relationships between soil moisture and fluorescence. Use of satellite-derived soil moisture and SIF measurements creates the opportunity for terrestrial ecosystem science that bridges water and carbon cycles.

The goals of this study were to advance the understanding of how SIF responds to soil moisture dynamics in the land surface model and to provide new insights into the relationship between carbon and water cycles. To achieve these goals, we updated SSiB2 to include a mechanistic representation of SIF. The SMOS soil moisture products were used to improve the soil moisture parameters, and finally, the SIF response to changing soil moisture was examined.

2. Materials and Methods

2.1. Ground and Satellite-Based SIF Measurements

The SIF field measurements were conducted at Harvard Forest (42.538°N, 72.171°W), which is a mixed temperate forest. This site is located in central Massachusetts, USA. The SIF measurements were collected from July to August in 2013. A novel system (FluoSpec) was developed to measure SIF at 760 nm in the field 5 m above the top of the forest canopy. A hyper spectrometer with a spectral resolution of ~0.13 nm between 680 and 775 nm (HR2000+, Ocean Optics, Inc.) was used. Based on the incident photosynthetically active radiation above the canopy (PAR_{above}), canopy-reflected PAR ($PAR_{reflect}$), and the average of understory PAR (PAR_{under}), which were all measured, the absorbed photosynthetically active radiation is calculated as follows:

$$APAR = PAR_{above} - PAR_{reflect} - PAR_{under} \tag{1}$$

And the SIF yield is given by

$$\text{SIF yield} = \text{SIF}/\text{APAR} \tag{2}$$

Details of the system and measurements were reported in Yang et al. (2015). Meteorological data, which were used as the SSiB2 forcing data, were available from the flux site measurements.

Global SIF data from GOSAT were used in this study. This satellite was launched on 23 January 2009. The satellite-based SIF data were derived based on high-resolution spectra covering Fraunhofer lines (narrow absorption features in the solar spectrum) in the 755–772 nm range. Details of the retrieval method and data descriptions can be found in Frankenberg, Butz, et al. (2011); Frankenberg, O'Dell, et al. (2011). We used global monthly 2° × 2° data to minimize the noise inherent in the original retrieval. The standard errors for GOSAT are 5–10% of the peak fluorescence, and the global average of the errors is smaller (Frankenberg, O'Dell, et al., 2011).

The monthly gridded SIF data products from the GOME-2 MetOp-A satellite were also used in this study. The data were archived onto a 0.5° grid. The GOME-2 MetOp-A satellite measured the spectrum for top-of-atmosphere radiance between 240 and 790 nm, and the data with wavelengths between 734 and 758 nm were used to estimate SIF. The level 3 GOME-2 SIF product was prescreened for clouds (≥30% cloud coverage were excluded). The footprint of the retrieval was approximately 40 km × 80 km before July 2013 and 40 km × 40 km since then. Since GOME-2 SIF was extracted for 740 nm, following Joiner et al. (2013) and Yang et al. (2015), GOME-2 SIF was multiplied with 0.582 to approximate SIF at 760 nm. The details of the retrieval method and data descriptions can be found in Joiner et al. (2013).

2.2. SSiB2 Model

The SSiB2 (Xue et al., 1991; Zhan et al., 2003) was used in this study. This model is a comprehensive land surface scheme that simulates the complex and heterogeneous interactions between land surface processes, hydrology, and the biosphere, including advanced treatments of the terrestrial CO_2 fluxes. An analytical solution from the model of Collatz et al. (1991) and Collatz et al. (1992) was developed and incorporated into SSiB2 (Zhan et al., 2003), which enhanced the model's ability to simulate land surface CO_2 fluxes. Moreover, since a big leaf type of model tends to produce a higher photosynthesis rate and greater evapotranspiration (Hari & Makela, 2003), a new scaling methodology for the canopy scale, which includes leaf-shading effects and takes diffuse radiation into account, has been developed in SSiB2, which is crucial to assessing the diffuse radiation "fertilization" effect.

2.3. Coupling the SIF Module With SSiB2

An existing fluorescence module, which was incorporated into the Community Land Model version 4 (CLM4, Lee et al., 2015), was incorporated into SSiB2. Some basic information for this fluorescence module is described in the supporting information (Test S1). The coupling of this module with SSiB2 enables the

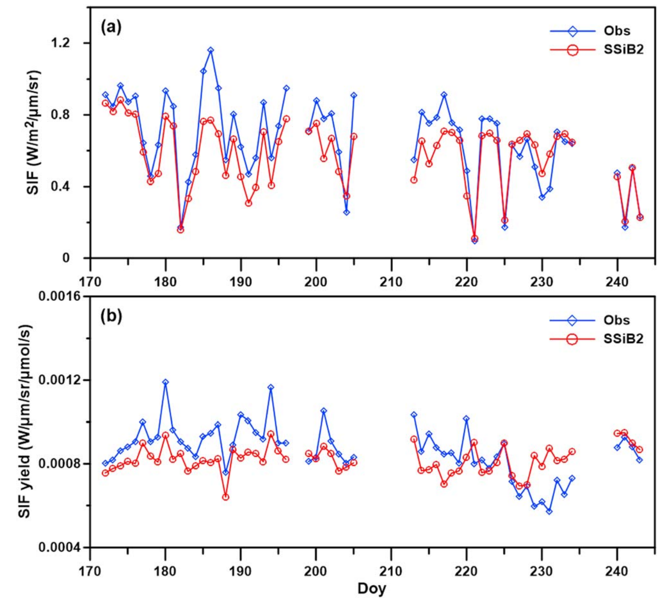

Figure 1. Daily mean solar-induced chlorophyll fluorescence (SIF) and SIF yield over the flux tower site at Harvard Forest, USA (42.538°N, 72.171°W). Blue line represents measured values over the flux tower, and red line represents the Simplified Simple Biosphere Model version 2.0 (SSiB2) result.

mechanistic representation of chlorophyll fluorescence, electron transport, and carboxylation, with light and moisture stress linked to photosynthetic activity and GPP. The parameterizations used for calculating photosynthesis in CLM4 are similar to those in SSiB2, thereby facilitating this coupling. The specific technical approach necessary to complete the coupling requires the tracking of the actual rate of electron transport from the SSiB2 photosynthesis parameterization to the potential rate of electron transport to the fluorescence module.

SSiB2 has been validated and evaluated using many observational data sets from different sites and vegetation types (Boone et al., 2009; Lokupitiya et al., 2016; Richardson et al., 2012; Rutter et al., 2009) and has been used in global and regional climate studies (Li et al., 2016; Xue et al., 2014). In this study, the performance of SIF simulations using SSiB2 was evaluated based on ground measurements. Hourly meteorological measurements collected at Harvard Forest were used as the forcing data for the SSiB2 model. The simulations covered the period from January to August in 2013. The first 6 months used as the spin-up time, and the results of the last two months were analyzed in this paper. Daily SIF was calculated as the mean value of field measurements collected between 6:00 a.m. and 6:00 p.m. We compared the daily mean SIF and SIF yield with field measurements from the Harvard Forest flux tower (Figure 1). The bias and root-mean-square error (RMSE) of SIF were 0.08 and 0.13 $W/m^2/\mu m/sr$, and SSiB2 captured the daily mean SIF reasonably well, indicating the capability of simulating SIF using this model. Figure 1b shows that the SIF yield simulated in SSiB2 was also close to the data with field measurements; the bias and RMSE were 0.00004 and 0.00012 $W/\mu m/sr/\mu mol/s$, respectively.

A spectrometer measured fluorescence as the power per solid angle, unit area, and wavelength range ($W/m^2/\mu m/sr$). Because SSiB2, similar to other land models, has only visible and near-infrared bands, to match the window of inversion of GOSAT SIF, the model values of fluorescence at the 757 nm wavelengths need to be estimated. We calculated the conversion factor from the Soil-Canopy Observations for Photosynthesis and Energy balance (SCOPE) model (Lee et al., 2015; van der Tol et al., 2009, 2014) to compare SSiB2 SIF with the measurements of GOSAT.

2.4. SMOS Soil Moisture Integration Into SSiB2

The SMOS mission, which was launched on 2 November 2009, is the European Space Agency's second Earth Explorer Opportunity mission. The primary goals of the SMOS mission were to globally and frequently measure the land surface soil moisture and sea surface salinity over the oceans (Kerr et al., 2001). Due to the progress in image reconstruction techniques, the operational retrieval algorithm was also improved and is able to discern surface soil moisture fields that fulfill the requirements over land (Kerr et al., 2016). The SMOS soil moisture data provide the best long-term record of global soil moisture currently available. The volumetric soil water content is used in this paper to describe the soil moisture. In general, the soil moisture spatial errors are low for SMOS, with a global average value of 0.023 m^3/m^3 (Kerr et al., 2016). The SMOS data were used to validate and evaluate the model soil moisture simulations.

The SMOS mission (Kerr et al., 2001, 2010) was the first mission designed for and dedicated to soil moisture and ocean salinity retrieval. The volumetric soil water content over land (0–5 cm) is measured globally and frequently. In SSiB2, the volumetric soil water content is calculated for three layers (the surface, the rooting zone, and the drainage zone). The soil moisture in the surface layer is calculated as follows:

$$\frac{\partial \theta_1}{\partial t} = \frac{1}{D_1}\left[P + Q_{12} - E_{gs} - b_1 E_{dc}\right] \tag{3}$$

where θ_1 is the volumetric soil water content, D_1 is the soil thickness of the surface layer, Q_{12} is the soil moisture change between the first and second layers, E_{gs} is evaporation from the soil surface, E_{dc} is transpiration from the surface layer, and b_1 is the root fraction in the first layer.

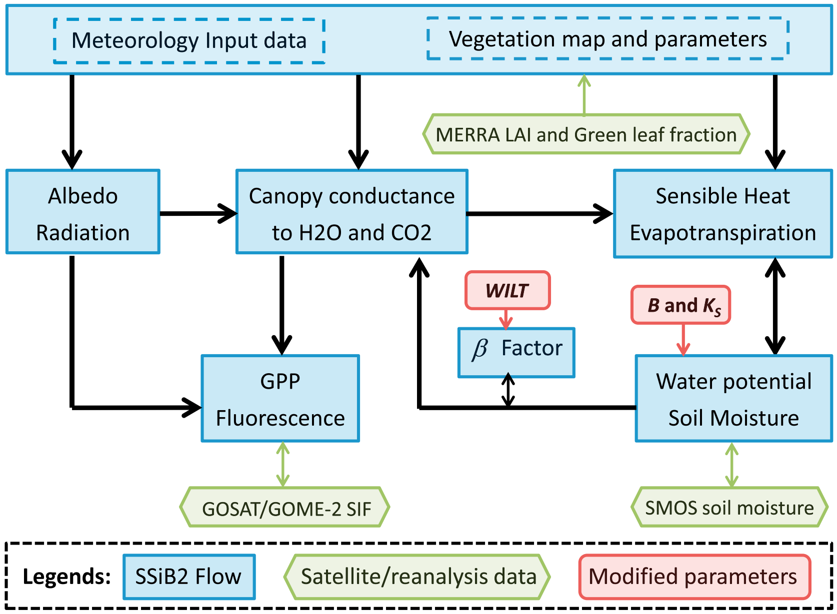

Figure 2. Overview flowchart of the Simplified Simple Biosphere Model version 2.0 (SSiB2) land surface model and the modified parameters in the model. The blue boxes are the SSiB2 flowchart; the green boxes are the satellite/reanalysis data; and the red boxes are the modified parameters in the model. GPP = gross primary production; MERRA = Modern-Era Retrospective Analysis for Research and Applications; LAI = leaf area index; GOSAT = Greenhouse gases Observing SATellite; GOME-2 = Global Ozone Monitoring Experiment-2; SMOS = Soil Moisture and Ocean Salinity.

In this paper, we used the SMOS data to validate and evaluate the SSiB2 surface soil moisture simulations. Although satellite-based soil moisture only reflects water in the top few centimeters of the soil, there is generally a strong relationship between soil moisture in the near-surface and soil moisture at greater depths. Ford et al. (2014) used in situ data from the U.S. Great Plains to evaluate the root zone soil moisture, which was derived from near-surface observations from SMOS. The results demonstrated that the near-surface soil moisture was closely related to the root zone soil moisture. In SSiB2, the surface layer is 2 cm for all soil types, but the soil thicknesses of the middle layers differ. Linear interpolation was used to derive the volumetric water content at 5 cm, which was compared with the SMOS data from the first and second layers. The differences were less than 0.005 m^3/m^3 for all plant functional types (PFTs) compared to the results of the first soil layer only.

2.5. Experimental Design

In this study, the offline two-dimensional SSiB2 simulations are driven with atmospheric forcing from the Princeton University Hydroclimatology Group Bias Corrected Meteorological Forcing Dataset (Sheffield et al., 2006). The time step of SSiB2 integration is 3 h, and the model is run at 1.0° × 1.0° spatial resolution. The experiments in this paper cover the period from 2008 to 2012. The first year is taken as a spin-up time, and the results of the last 4 years are analyzed.

Figure 2 shows the overview flowchart of SSiB2 and the satellite data. The blue boxes are the SSiB2 and SIF model components, and the green boxes are the satellite or reanalysis products. These products were used as benchmarks to adjust the parameters and to evaluate the model simulation against the GOSAT and SMOS products or were used as model input for simulation, such as the National Aeronautics and Space Administration Global Modeling and Assimilation Office's Goddard Earth Observing System Data Assimilation System version 5 Modern-Era Retrospective Analysis for Research and Applications (MERRA) data set (Rienecker et al., 2011). The red boxes show parameters modified in the experiment. In section 4, this flowchart will be discussed comprehensively. Table 1 lists the experimental design of this study.

In SSiB2, the leaf area index (LAI) and green leaf fraction of each PFT were derived based on ground survey and limited satellite information (Dorman & Sellers, 1989; Xue, Zeng, et al., 1996), which contain substantial uncertainties. In the control run (referred to as CTL hereafter), these original data sets were used for the

Table 1
Experimental Design

	Experiment description
CTL	The original LAI, green fraction, and vegetation cover fraction
Test Veg	With modified LAI, green leaf fraction, and cover fraction
Test Veg+Soil	Same as Test Veg but *B* parameter and hydraulic conductivity at saturation are modified
Test Veg+Soil+WILT	Same as Test Veg+Soil but wilting point is modified

model simulation as a benchmark run. As both the LAI and green leaf fraction are important parameters in the land surface model, especially for the calculation of photosynthesis, and have a substantial effect on the model simulation of the hydrological cycle (Kang et al., 2007), in the Test Veg run (referred to as Test Veg hereafter), the monthly mean MERRA LAI and green leaf fraction were applied to assess their impact on carbon simulation. As their impacts were large, in the two subsequent sensitivity tests (Test Veg+soil run and Test Veg+soil+WILT run), we also used the MERRA LAI and green leaf fraction to obtain a more realistic estimation of the terrestrial surface carbon flux and its sensitivity to model parameters.

The vegetation-soil layer affects the radiative transfer at the surface and the partitioning of surface energy into sensible and latent heat fluxes. Studies have shown that soil properties can have a substantial impact on model simulations of surface hydrology. However, values for a number of the parameters are scarce for different types of vegetation in the world (Kahan et al., 2006; Xue, Zeng, et al., 1996). Roughly estimated parameter values cause uncertainty in land surface model simulations. To identify parameters that affect both carbon cycles and soil moisture, GOSAT and SMOS satellite data were introduced as constraints to adjust the land model parameters to ensure more realistic simulations of surface water and carbon cycles in this paper. The satellite data provide a new approach to obtain a better global view of carbon flux and soil moisture.

Since SSiB2 includes numerous vegetation and soil parameters, we first conducted preliminary sensitivity experiments and statistical analyses to identify the most important parameters for the soil moisture simulation. A global sensitivity analysis algorithm known as the extended Fourier Amplitude Sensitivity Test (EFAST) was applied to identify the key parameters for soil moisture simulation using the SSiB2 land surface model. EFAST is a global and quantitative sensitivity analysis algorithm that can be used for land surface models that are complex, nonlinear, and nonmonotonic (Saltelli et al., 1999, 2010). The sensitivity index of each parameter can be derived from the analysis of the impacts of the input factors on the output variance. Therefore, EFAST is highly efficient and accurate and takes into account the interactions among parameters. Some basic information pertaining to the EFAST algorithm is described in the supporting information (Test S2).

The objective is to generate a matrix of results corresponding to different input variable settings based on the SSiB2 vegetation and soil parameter range (Dorman & Sellers, 1989; Sellers et al., 1996). The input parameters in the SSiB2 land surface model are listed in Table S1, and the descriptions for the vegetation types are listed in Table S2. In this paper, we define the areas that are covered by savannah, grasslands, and shrub (vegetation types 6 to 9 in SSiB) as semiarid regions. A total of 2210 combinations was used in the EFAST test to evaluate the direct and interactive effects. The method efficiently quantifies the relative effects of input variables on model output through the use of the main sensitivity index (S_i) and the total sensitivity index (ST_i). Different PFTs may have different characteristics of the parameter sensitivities of simulating soil moisture. In this paper, the key parameters were identified among the different vegetation types. The sensitivity index results for soil moisture for four typical vegetation types are shown in Figure S1. Despite the large number of SSiB2 input variables, the S_i and ST_i results identify a few parameters that have a large impact on soil moisture. It was observed that two key parameters, *B* parameter and hydraulic conductivity at saturation (K_s), had the larger impacts than the other parameters. The impact of the wilting point on the soil moisture simulations was lower than that of the *B* parameter and K_s but still substantially larger than that of the other parameters.

These three key parameters were selected for further calibration. In the Test Veg+Soil run (referred to as Test Veg + Soil hereafter), the *B* parameter, which affects the conversion from soil moisture to soil water potential and subsequently the soil moisture diffusion between different soil layers, and hydraulic conductivity at saturation (K_s) were modified in the model. In the Test Veg+Soil+WILT run (referred to as Test Veg+Soil+WILT hereafter), the wilting point, the *B* parameter, and K_s were adjusted. Because of the large uncertainty in these parameters, they have been calibrated in a number of studies based on the scale of investigation to produce results close to observations (Xue, Zeng, et al., 1996; Zhang et al., 2015).

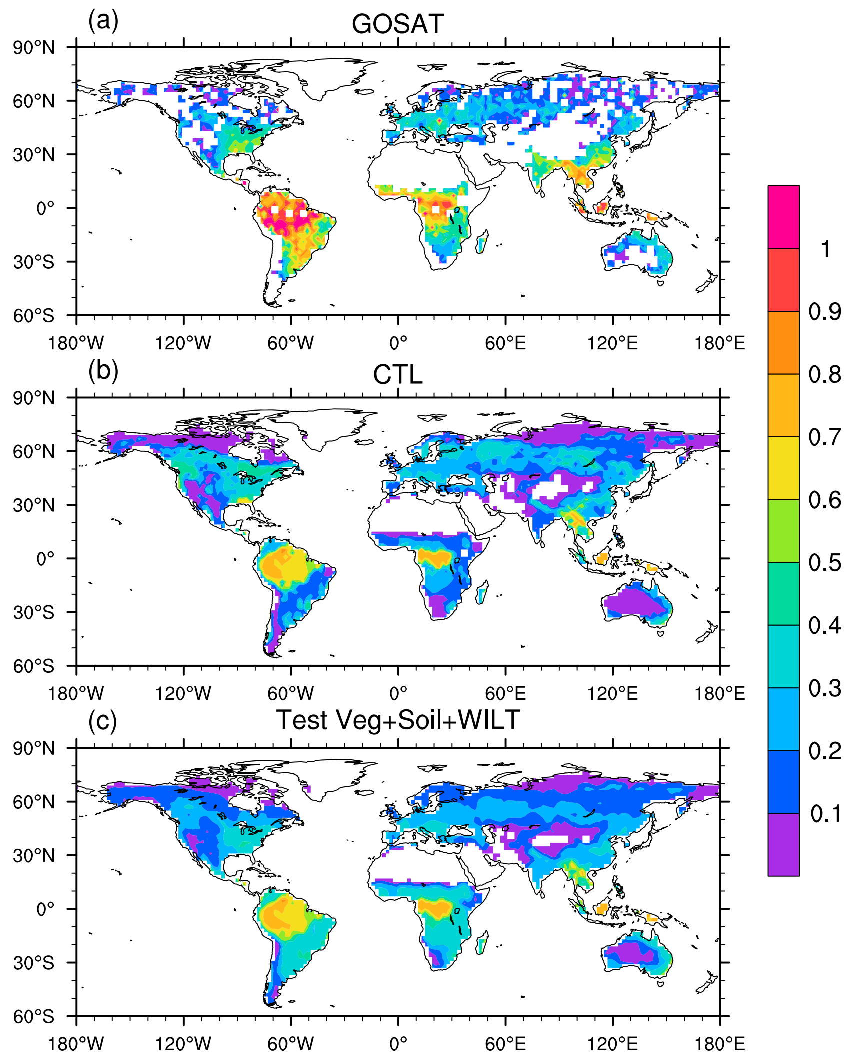

Figure 3. Global map of annual mean solar-induced chlorophyll fluorescence (SIF) from 2009 to 2012, units: W/m^2/μm/sr. (a) Greenhouse gases Observing SATellite (GOSAT), (b) control run (CTL), and (c) Test Veg+Soil+WILT.

This study mainly focused on the multiyear averages of soil moisture, SIF, and GPP in the SSiB2 model. The simulations were compared to satellite products. To quantify the simulating ability of the SSiB2, three common statistical measures, namely, the spatial correlation coefficient (SCC), the mean bias (BIAS), and the RMSE, were calculated in this study.

3. Results

Table 1 lists the different experiments discussed in the previous section. This section discusses the main results of these experiments. The global SIF results from the GOSAT measurements and the SSiB2 land surface model simulation using original LAI data (Dorman & Sellers, 1989) are compared in Figure 3. The simulated SIF has a spatial pattern similar to that of the GOSAT SIF, but the values are lower in most areas. This bias was likely caused by the inaccuracy of the LAI and the green leaf fraction. To obtain a more realistic SIF simulation, the MERRA LAI and green leaf fraction were used in the experiment, referred to as Test Veg in this paper. The vegetation cover fraction was also adjusted based on the satellite data (Kang et al., 2007). The global differences in annual mean SIF compared to GOSAT and GOME-2 data are shown in Figure 4. The SIF in CTL shows a negative bias in most parts of the Southern Hemisphere, India, and Southeast China but a positive bias in boreal forest areas and Eurasian steppes (Figures 4a and 4b). The simulated SIF improved in Test Veg (Figures 4c and 4d). The results showed that the simulated SIF was improved compared to both GOSAT and GOME-2 data. The SSiB2 simulated SIF decreased in the high latitudes of the Northern Hemisphere

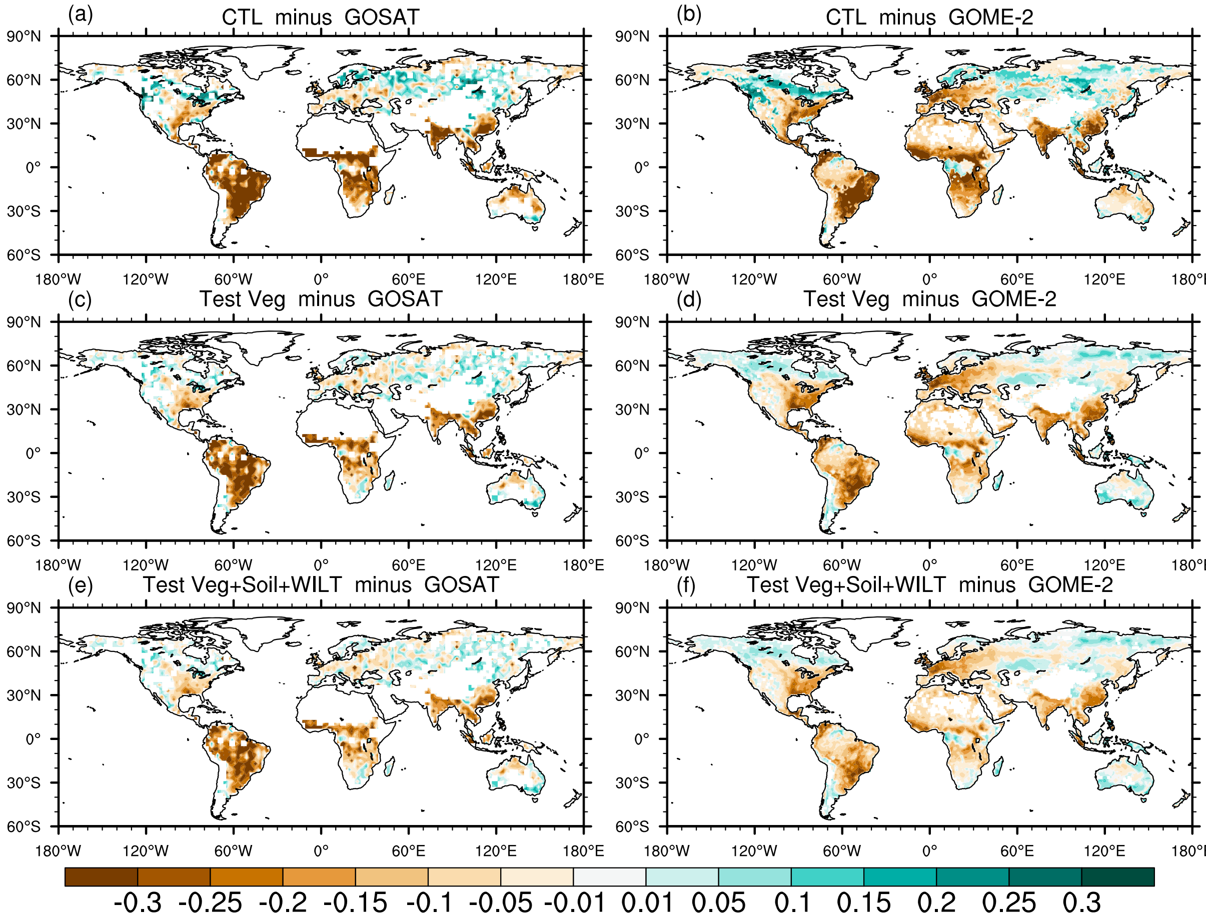

Figure 4. Global differences of annual mean solar-induced chlorophyll fluorescence compared to Greenhouse gases Observing SATellite (GOSAT) and Global Ozone Monitoring Experiment-2 (GOME-2) data, units: W/m^2/μm/sr. (a) CTL minus GOSAT, (b) CTL minus GOME-2, (c) Test Veg minus GOSAT, (d) Test Veg minus GOME-2, (e) Test Veg+Soil+WILT minus GOSAT, and (f) Test Veg+Soil+WILT minus GOME-2.

and increased in South America, western and southern Africa, and India after more realistic LAI and green leaf fraction data sets were used. Table 2 shows the SCCs, BIASs, and RMSEs of simulated global SIF with respect to the GOSAT observations. The SCC of Test Veg increased by 31% compared to that in CTL. Both experiments showed a negative bias, but in Test Veg, the bias was reduced by 21%. The RMSE of Test Veg was reduced by 16%. These results confirm those from a multimodel intercomparison, indicating that models specified with improper representations of phenology have difficulty in producing adequate surface carbon flux (Richardson et al., 2012). In the following analyses, Test Veg, which employed the more realistic LAI, was used as a base run for comparison with other experiments.

Soil moisture and the parameterization of its transfer within soil layers are key elements in SSiB (Xue, Zeng, et al., 1996) and affect carbon exchange between the soil and air (Zhan et al., 2003). To understand the relationships between soil moisture and carbon cycling, we compared soil moisture from the SMOS mission and Sun-induced fluorescence data from GOSAT and GOME-2 with the SSiB2 results to evaluate the global impacts of various simulated soil moisture values on carbon budgets. This approach included an investigation of the model parameter uncertainties using a set of parameter values within the uncertainty range. We compared the model simulations with satellite measurements to yield the best model parameters leading to the closest match against the SMOS, GOSAT, and GOME-2 measurements, which is the ultimate objective of our model development—improved model performance against benchmark measurements within a physically realistic parameter range.

Table 2
Spatial Correlation Coefficient (SCC), Mean Bias (BIAS), and Root-Mean-Square Error (RMSE) of SIF Compared to the GOSAT Data, Unit: W/m^2/μm/sr

	CTL	Test Veg
SCC	0.54	0.71
BIAS	−0.09	−0.07
RMSE	0.26	0.21

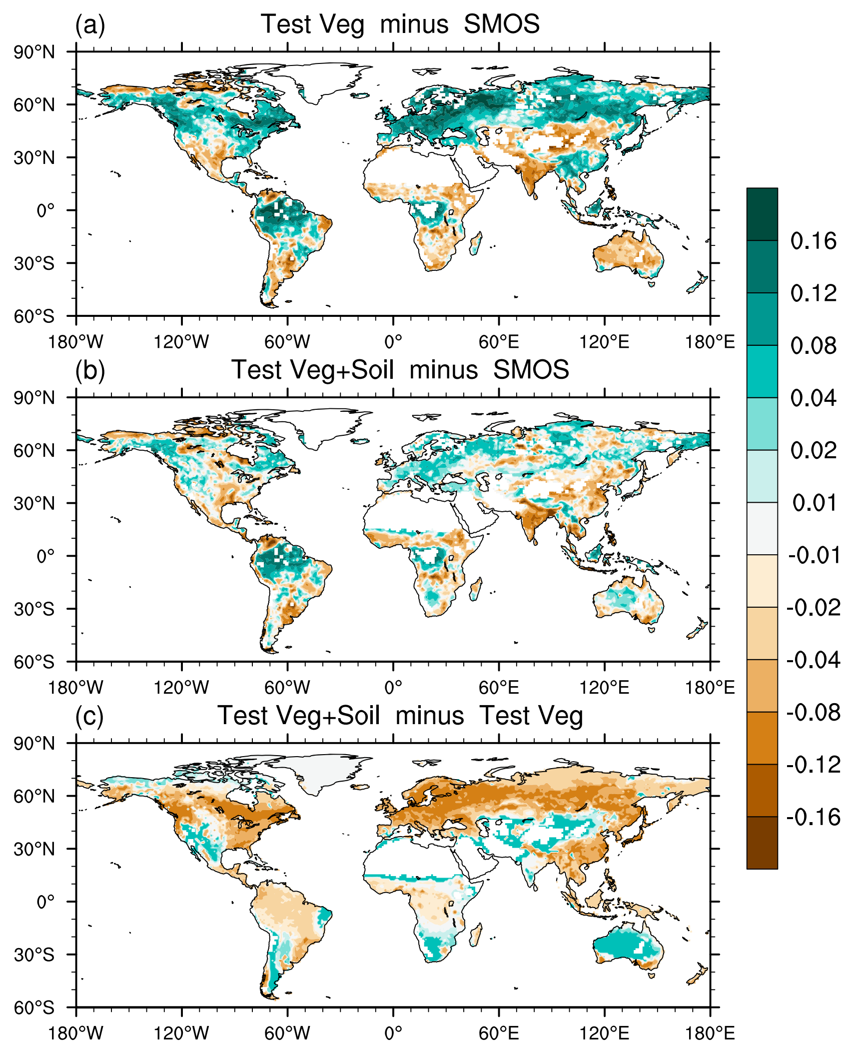

Figure 5. Global difference of soil moisture, units: m^3/m^3. (a) Test Veg − Soil Moisture and Ocean Salinity (SMOS), (b) Test Veg+Soil − SMOS, (c) Test Veg+Soil − Test Veg.

Reliable parameter values for these three parameters are not available, and there are uncertainties in inputting values for these parameters in the model (Xue et al., 1997); consequently, similar studies have been carried out to identify important soil parameters in surface hydrology (Xue, Zeng, et al., 1996). Among the soil parameters, K_s and the B parameter have been identified to significantly affect the simulation of soil moisture. Both parameters influence the soil moisture simulation by affecting the soil hydraulic conductivity, field capacity, and subsequently the soil moisture diffusion processes. In addition, the wilting point also has an impact on soil moisture through its influence on stomatal conductance and consequently transpiration. We report the experiments that tested these three parameters (Table 1) and their results in this paper.

The SMOS data were used as a benchmark to adjust K_s and the B parameter in Test Veg+Soil. The original and new values of K_s and the B parameter are shown in the supporting information (Table S3). Figure 5 shows the global difference between the simulation and SMOS data and between the different experiments for soil moisture. In Test Veg, the boreal forest, tropical areas, and southeast China had positive biases, and different degrees of negative biases can be seen in other areas (Figure 5a). In Test Veg+Soil, we used the SMOS data to calibrate K_s and the B parameter to obtain better results. The soil moisture in Test Veg+Soil increased/decreased in areas with negative/positive bias in Test Veg (Figure 5b). This result indicates that after parameter calibration using satellite data, the simulated soil moisture improved. Figure 6 shows that after calibration, the global soil moisture RMSE had a substantial reduction, by 22%. In addition, SCC

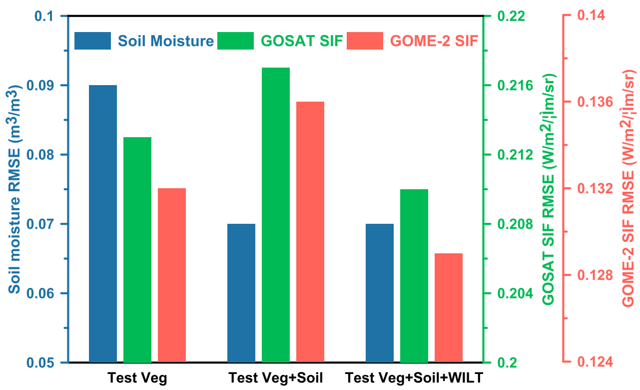

Figure 6. Global root-mean-square error (RMSE) of different experiments relative to Soil Moisture and Ocean Salinity (SMOS) soil moisture and Greenhouse gases Observing SATellite (GOSAT) and Global Ozone Monitoring Experiment-2 (GOME-2) solar-induced chlorophyll fluorescence (SIF).

increased by 19%. Applying global-scale satellite observations of soil moisture, such as the SMOS product, is an effective approach to improve the ability of this land surface model to simulate soil moisture.

In addition to the SMOS data, the GOSAT and GOME-2 SIF provide a new method to check whether the model's representation of photosynthesis processes is improved. The analysis of the Test Veg+Soil results, however, showed that although soil moisture was better simulated following the calibration of the soil parameters, the simulated SIF results, compared against the GOSAT and GOME-2 SIF product, were substantially worse (Figure 6). Nevertheless, the change in SIF in Test Veg+Soil confirmed that the changes in soil moisture had substantial impacts on photosynthesis processes. We have since conducted a number of sensitivity studies and identified that the wilting point, which is the minimum soil moisture at which a plant loses turgidity and can no longer recover, is a crucial parameter for better SIF simulation under adequate soil moisture. After calibration of the wilting point, the simulated global SIF in Test Veg+Soil+WILT improved substantially compared against the GOSAT and GOME-2 SIF product and retained reasonable simulations for soil moisture (Figure 6). The annual mean SIF for Test Veg+Soil+WILT from 2009 to 2012 is shown in Figure 3c. The global differences between the simulations and the satellite (GOSAT and GOME-2) data are shown in Figures 4e and 4f, respectively.

Studies have shown that satellite-retrieved SIF provides useful information on terrestrial photosynthesis and GPP (Frankenberg, O'Dell, et al., 2011; Lee et al., 2015). We also investigated whether the land surface model could better simulate GPP after the improvements in the SIF simulation, which would further confirm the close relationship between SIF and GPP. We applied the Max Planck Institute for Biogeochemistry (MPI-BGC) GPP product from the FLUXNET-based Model Tree Ensemble (MTE) (Beer et al., 2010) as the benchmark in this study. Figure 7 shows the global differences in annual mean GPP from all of the experiments compared to the MPI-BGC products. The global GPP in CTL (Figure 7a) shows a negative bias in magnitude, especially in South America and most of Africa. In the high latitudes of the Northern Hemisphere, the modeled GPP was slightly higher compared to the MPI-BGC product, consistent with the SIF results shown in Figure 4. In Test Veg (Figure 7b), the simulated GPP improved after the MERRA LAI and green leaf fraction were used. However,

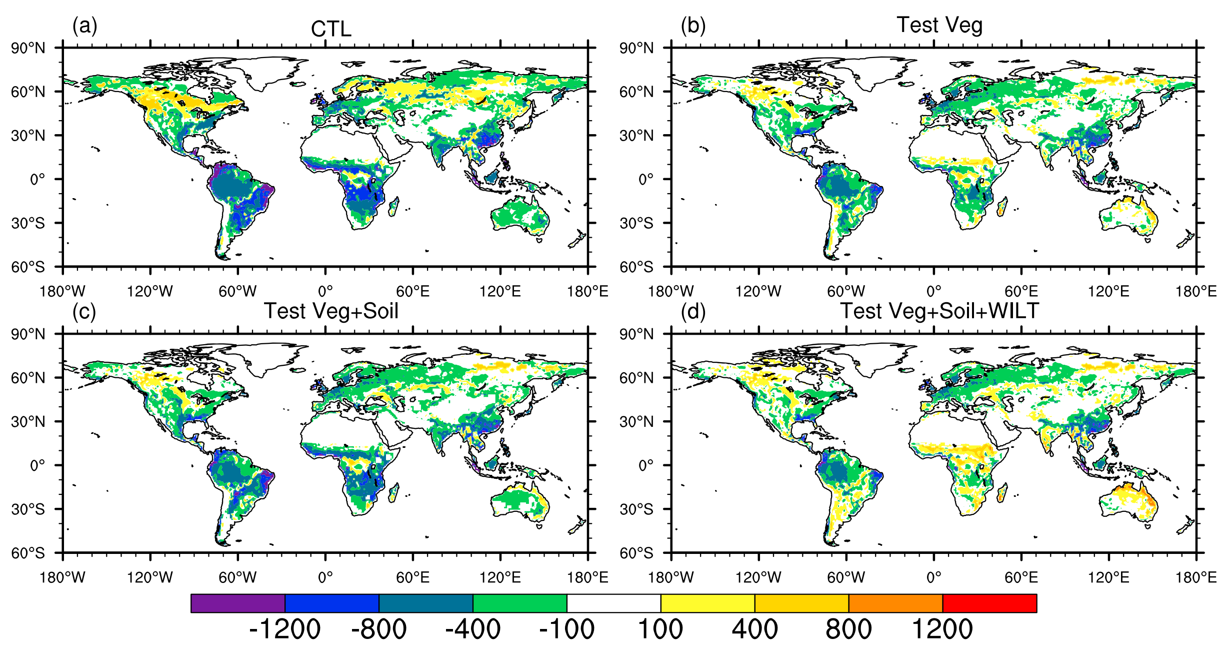

Figure 7. Global difference of gross primary production between MPI-BGC and the experiments, units: g C/m^2/yr. (a) Control run (CTL), (b) Test Veg, (c) Test Veg+Soil, (d) Test Veg+Soil+WILT.

Table 3
Mean Bias (BIAS), Spatial Correlation Coefficient (SCC), and Root-Mean-Square Error (RMSE) of GPP Compared to the MPI-BGC Data, Unit: g C/m^2/yr

	SCC	BIAS	RMSE
CTL	0.84	−246	504
Test Veg	0.91	−146	365
Test Veg + Soil	0.89	−224	429
Test Veg + Soil+WILT	0.90	−80	357

when SSiB2 produced better simulated soil moisture in Test Veg+Soil (Figure 7c), the GPP simulation worsen. After the calibration of the wilting point, the global GPP in Test Veg+Soil+WILT (Figure 7d) improved substantially. The model simulations still showed large biases in the Amazon, northern Europe, and China. The land surface model consists of many processes, and further investigations are needed to understand and improve these processes. Although the simulated GPP spatial distribution from different cases showed similar spatial patterns (Figure 7), the parameters' impacts on GPP were substantial. Table 3 shows the SCCs, BIASs, and RMSEs of the global simulated GPP from different experiments. The MERRA LAI and green fraction had a substantial impact on the GPP simulation: the SCC increased by 8% in Test Veg compared to CTL, and Bias and RMSE were reduced by 41% and 28%, respectively (Table 3). However, the bias and RMSE were worse in Test Veg+Soil compared with Test Veg, similar to the SIF results. The GPP simulation in Test Veg+Soil+WILT was the best among the four experiments and was, consistent with the results in which SIF was used as a benchmark for comparison.

This study shows that the wilting point is a key parameter linking soil moisture and photosynthesis; tests indicated that the sensitivity of GPP to the wilting point varies among vegetation types. Figure 8 shows the RMSEs for the vegetation types that had substantially improved GPP simulations after the wilting point was calibrated. As discussed before, without the wilting point calibration, the results would be deteriorated substantially. The RMSE of SIF was calculated at global scale. However, the wilting point has larger impacts on the SIF simulations over semiarid region. Table 4 showed that the RMSE of SIF and GPP in Test Veg+Soil was increased by 18% and 32%, respectively, compared to the values in Test Veg+Soil+WILT. This suggests that the wilting point is more important in connecting the carbon and water cycles in semiarid regions. The soil water condition is a limited factor for vegetation growth in semiarid regions, where the soil moisture is approaching and crossing the wilting point more frequently.

4. Discussion

Sun-induced chlorophyll fluorescence provides a new approach to quantify photosynthetic efficiency (Flexas et al., 2002). Lee et al. (2015) incorporated SIF into photosynthesis parameterization in the National Center for Atmospheric Research (NCAR) CLM4 land surface model and demonstrated its utility as a diagnostic tool for the evaluation of modeled photosynthesis, which is one of the key processes in land surface modeling that strongly influence the carbon, water, and energy balance. Lee et al.'s paper mainly focused on SIF coupling with the NCAR CLM4 land surface model, and the relationships between SIF and soil moisture were not discussed. It should be noted that our approach would also improve the rooting zone soil moisture. The MERRA data include the surface soil moisture (0–2 cm) and root zone soil moisture (0–100 cm). Using the approach discussed in this paper, the adjustment of K_s and the B parameter using the surface soil moisture, the simulations of root zone soil moisture also improved in SSiB2 as shown in Table S4.

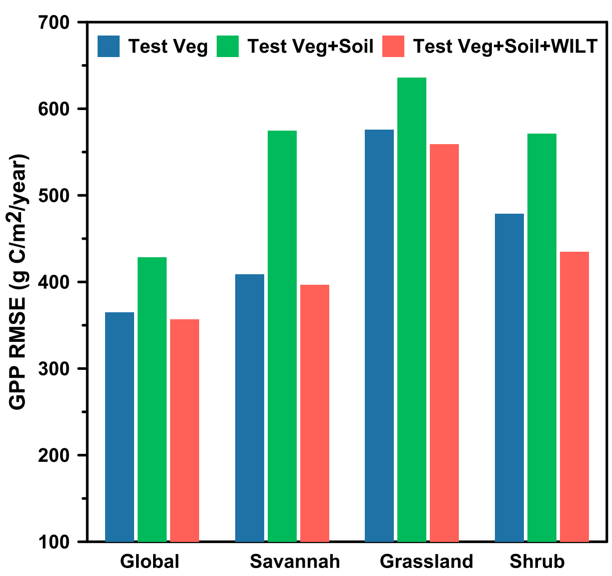

Figure 8. Root-mean-square error (RMSE) of gross primary production (GPP) from different vegetation types, units: g C/m^2/yr.

The seasonal soil moisture, SIF, and GPP in the three experiments were calculated at global scales (Figure 9). The soil moisture simulations improved after adjusting the B parameter and K_s, but SIF and GPP worsened for throughout the year. However, the SIF and GPP simulations improved after modifying the wilting point in the model and the simulations for soil moisture retained reasonable. The most improvements for soil moisture were from March to September and for SIF and GPP were from June to August, when the photosynthesis process was quite strong in Northern Hemisphere.

To understand carbon-water cycles and the roles of some important parameters involved in this coupling, we further examined the soil

Table 4
Root-Mean-Square Error of Solar-Induced Chlorophyll Fluorescence (SIF) and Gross Primary Production (GPP) Compared to the Global Ozone Monitoring Experiment-2 and MPI-BGC Data in Semiarid Regions, Unit: SIF (W/m^2/μm/sr), GPP (g C/m^2/yr)

	SIF	GPP
Test Veg+Soil+WILT	0.11	352
Test Veg+Soil	0.13	464

and photosynthesis parameterizations in SSiB2 (Xue, Fennessy, et al., 1996; Zhan et al., 2003). Figure 2 shows the overview flowchart of the SSiB2 land surface model and the modified parameters. There are three soil layers in the calculation of soil moisture. The gradient of soil water potential is used to calculate the diffusion of soil water, and it is defined as follows:

$$\psi = \psi_s \left(\frac{\theta}{\theta_s}\right)^{-B} \tag{4}$$

where the B parameter is an empirical constant that is dependent on the soil type and θ_s is the volumetric soil water content at saturation. The soil water diffusion equation is written as follows:

$$Q = -k_s \left(\frac{\theta}{\theta_s}\right)^{(2B+3)} \left[\frac{\partial \psi}{\partial Z} + 1\right] \tag{5}$$

where Q is proportional to the soil water conductivity at saturation. Because of their roles in the soil moisture diffusion, it is not surprising that the calibration of B and K_s has a substantial impact on the soil moisture simulation. The canopy stomatal resistance, r_c, used for transpiration and carbon assimilation is closely related to soil moisture. Studies (Blackman & Davies, 1985) have indicated that the stomatal response to the water supply is controlled by soil water potential and that roots "sense" the soil moisture supply and directly transmit chemical messages to the guard cells to adjust stomata opening. In SSiB2, stomatal opening is controlled by soil moisture through the β factor:

$$\beta = 1 - \exp\{-C_2[C_1 - \ln(-\psi)]\} \tag{6}$$

where C_1 is the natural logarithm of the wilting point. In the model, the stomata close completely at the wilting point. C_2 is a slope factor that depends on the vegetation type. The wilting point is directly linked to stomatal resistance (or conductance, the reciprocal of resistance) and consequently to transpiration and photosynthesis processes. The wilting point affects soil moisture through transpiration. Our experiments show that the impact of the wilting point on soil moisture is not as efficient as that of K_s and the B parameter. The wilting point has a direct impact on the photosynthesis process through the β factor, but B and K_s influence this factor through the soil water potential.

In most semiarid regions, the simulated soil moisture (Figure 6) was lower compared with the SMOS product, and the SIF (Figure 4b) and GPP (Figure 7b) also exhibited negative biases. Calibration of B and K_s resulted in a close match between soil moisture and the SMOS products; however, this modification also affected the β factor and subsequently stomatal resistance, which resulted in poorer simulations for SIF and GPP. To overcome this problem, the wilting point was calibrated in equation (6) using SMOS data to generate an appropriate β factor. The original and new values of the wilting point are shown in the supporting information (Table S5). Although the above discussion is based on SSiB2, the soil moisture diffusion equations based on Darcy's law and Clapp and Hornberger (1978) are widely used in land surface models, and the parameterization

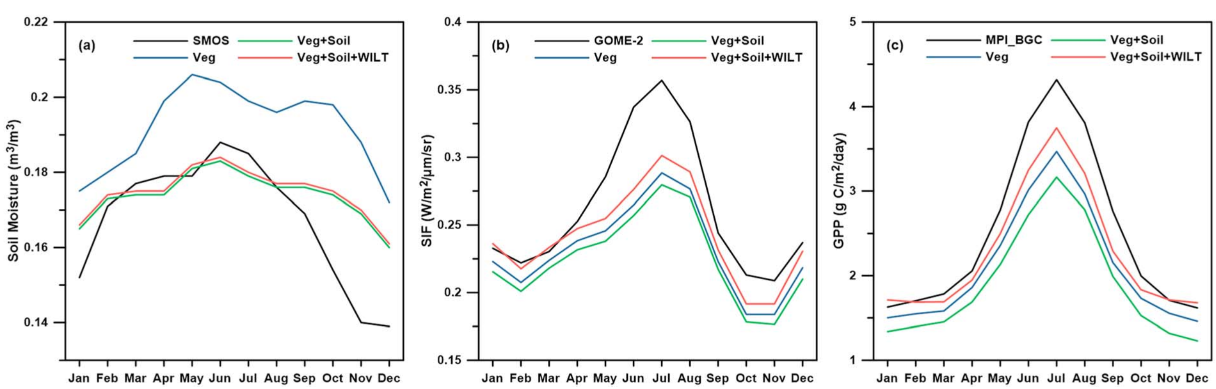

Figure 9. The monthly mean (a) soil moisture, (b) solar-induced chlorophyll fluorescence, and (c) gross primary production at the global scale in Test Veg, Test Veg+Soil, and Test Veg+Soil+WILT. SMOS = Soil Moisture and Ocean Salinity.

Table 5
Soil Parameters Used in the Experiments

	B parameter	K_s	Wilting point[a]
Experiment A	5, 6, 7, 8, 9	2E-5	6
Experiment B	7	2E-3, 2E-4, E-5, 2E-6, 2E-7	6
Experiment C	7	2E-5	4, 5, 6, 7, 8

[a]The values are the logarithm of negative soil water potential for wilting point.

of the link between the wilting point and stomatal resistance is also applied in many models with various forms (Niu et al., 2011).

Several experiments have been conducted to determine model sensitivity to changes in different parameters. For example, two vegetation types, savanna and grassland, were chosen, and sensitivity tests were driven using atmospheric forcing data from the bias-corrected meteorological forcing data set of Princeton University's Hydroclimatology group (Sheffield et al., 2006). The experiments covered the period from 2009 to 2010. The first year was used as the spin-up time, and the results for summer in 2010 were analyzed. Table 5 lists the values of the soil parameters used for experiments A, B, and C and the ranges of the *B* parameter, K_s, and the wilting point, respectively. The changes for each parameter are within the normal range of soil and vegetation property variations (Xue, Zeng, et al., 1996).

Figures 10a and 10b show that the soil wetness increased with a higher *B* parameter (from sandy to clay texture) because an increase in the *B* parameter value reduces soil hydraulic conductivity (equation (5)) and increases soil wetness. The SIF and GPP values decreased with an increase in the *B* parameter. An increase in K_s (from clay to sandy texture) resulted in a decrease in soil wetness and an increase in SIF and GPP (Figures 10b and 10d). For most of the semiarid regions, both the simulated soil moisture and SIF values were lower compared with the satellite data. After the *B* parameter and K_s were modified to result in greater soil moisture, the simulated SIF and GPP values decreased and worsened as shown in Test Veg+Soil (Figure 6). Figures 10e and 10f show that a higher wilting point decreases soil wetness, but this change was not very large, unlike that resulting from modifications of the *B* parameter and K_s. However, SIF and GPP increase substantially with an increase in the wilting point because of the direct impacts on the calculation of the β factor (equation (6)). The results show that the wilting point strongly affects the photosynthetic process but does not alter soil moisture. As such, after calibrating the three parameters, the soil moisture, SIF, and GPP simulations improved.

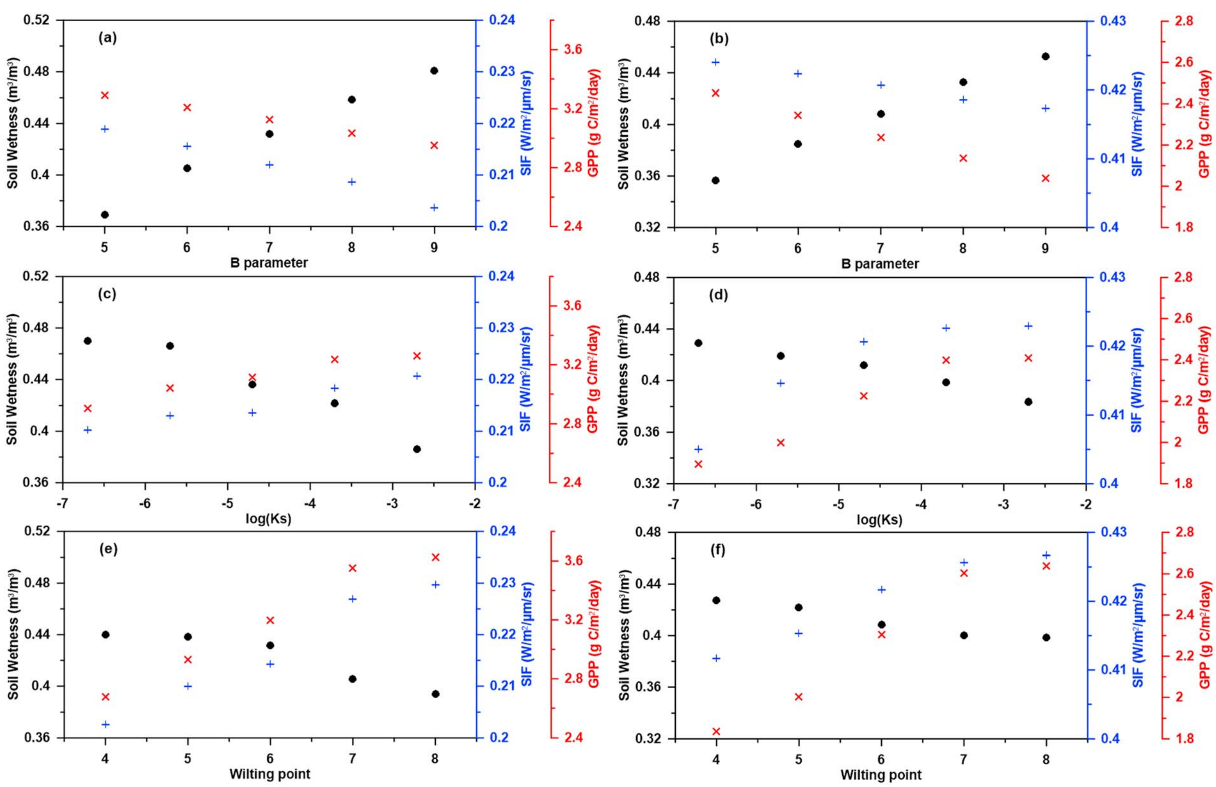

Figure 10. Calculated soil moisture (black), solar-induced chlorophyll fluorescence (SIF) (blue), and gross primary production (GPP) (red) for savannah (a, c, and e) and grassland (b, d, and f), (a and b) *B* parameter; (c and d) logarithm of K_s; (e and f) wilting point.

This study confirms the close relationship between soil moisture and terrestrial carbon processes, which are linked through the wilting point. It is important to adequately represent and dynamically couple both processes to ensure a comprehensive understanding of water and carbon cycles. With the previously launched OCO-2 (Frankenberg et al., 2014), the Sentinel-5 Precursor/TROPOspheric Monitoring Instrument (Guanter et al., 2015), and the proposed FLuorescence EXplorer (FLEX) (recommended for the European Space Agency explorer 8 mission) (Rascher et al., 2015), improved SIF measurements with higher spatial and/or temporal resolution, higher signal-to-noise ratio, and/or increased spectral bands (e.g., the added red emission peak near 680 nm in FLEX) are expected.

The launched Soil Moisture Active Passive mission is National Aeronautics and Space Administration's first Earth-observing satellite mission designed to provide continuous global observations of surface soil moisture. Aquarius, which launched on 10 June 2011 and was operational until 7 June 2015, focused on salinity retrieval from radiometric measurements in the L-band and has also shown the ability to deliver soil moisture products (Bindlish et al., 2015).

Forthcoming work will integrate Soil Moisture Active Passive soil moisture and fluorescence from OCO-2, which can provide products of better quality, spatial and temporal resolution, coverage, accuracy, and precision, as further constraints and coupling between the water and carbon cycles are developed. These data sets along with existing soil moisture and SIF data will pave the way for satellite observations leading to advances in the predictive understanding of global terrestrial coupled carbon-water cycles.

Although SIF simulations have improved for semiarid regions, large errors still exist. In this paper, we just focused on the relationship between soil moisture and SIF; some other important factors, such as the canopy structure and Rubisco V_{cmax} (Lee et al., 2015; Verrelst et al., 2015), were not included in this paper. In the further work, we will continue to include these factors to have better SIF simulations in SSiB model.

5. Conclusions

In this paper, we used SMOS, GOSAT, and GOME-2 data observations within the framework of SSiB2 to investigate how SIF responds to changing soil moisture and to identify the key parameter of carbon-water cycles. This study shows that although calibration of K_s and the B parameter in the SSiB2 model resulted in better soil moisture simulations, the SIF and GPP simulations were poorer. To overcome this issue, it was necessary to calibrate another parameter, the wilting point, to improve both global SIF and GPP. This research focuses on the integration of both a key water cycle variable—soil moisture (from SMOS)—and a key carbon cycle variable—chlorophyll fluorescence (from GOSAT and GOME-2), which also has a direct link to the total gross amount of carbon taken up by plants. This study demonstrates the close link between the water and carbon cycles in the application of remote sensing data and the SSiB2 land surface model.

Acknowledgments
This work was supported by NASA Jet Propulsion Laboratory Strategic University Research Program (SURP) grant 1514518, National Science Foundation grants AGS-1419526 and AGS-1346813, Natural Science Foundation of China (41475063, 41705056), the Natural Science Foundation of Jiangsu Province (BK20170638), and the International Cooperation and Exchange Programs of National Science Foundation of China (Sino-German, 41761134082). J. B. F. was also supported in part by NASA's IDS, SUSMAP, INCA, and CARBON programs. This work is also supported by the Jiangsu Collaborative Innovation Center for Climate Change. The authors thank Christian Frankenberg of the Jet Propulsion Laboratory for providing the GOSAT SIF data and Professor Jung-Eun Lee of Brown University for providing CLM4 model for our reference. The authors acknowledge the European Space Agency (Project AO-3230) for providing the SMOS data and the National Aeronautics and Space Administration for the MERRA data sets. The Harvard Forest SIF data are available at http://harvardforest.fas.harvard.edu:8080/exist/apps/datasets/showData.html?id=hf283. The model forcing data are available at http://hydrology.princeton.edu/data/pgf/1.0deg/3hourly/. The authors appreciate Matt Zebrowski of UCLA's technical assistance for this article. J. B. F. contributed to this research at the Jet Propulsion Laboratory, California Institute of Technology, under a contract with the National Aeronautics and Space Administration, California Institute of Technology. Government sponsorship is acknowledged.

References

Baker, N. R. (2008). Chlorophyll fluorescence: A probe of photosynthesis in vivo. *Annual Review of Plant Biology*, *59*(1), 89–113. https://doi.org/10.1146/annurev.arplant.59.032607.092759

Beer, C., Reichstein, M., Tomelleri, E., Ciais, P., Jung, M., Carvalhais, N., et al. (2010). Terrestrial gross carbon dioxide uptake: Global distribution and covariation with climate. *Science*, *329*(5993), 834–838. https://doi.org/10.1126/science.1184984

Bindlish, R., Jackson, T., Cosh, M., Zhao, T., & O'neill, P. (2015). Global soil moisture from the Aquarius/SAC-D satellite: Description and initial assessment. *IEEE Geoscience and Remote Sensing Letters*, *12*(5), 923–927. https://doi.org/10.1109/LGRS.2014.2364151

Blackman, C. J., Brodribb, T. J., & Jordan, G. J. (2009). Leaf hydraulics and drought stress: Response, recovery and survivorship in four woody temperate plant species. *Plant, Cell & Environment*, *32*(11), 1584–1595. https://doi.org/10.1111/j.1365-3040.2009.02023.x

Blackman, P., & Davies, W. (1985). Root to shoot communication in maize plants of the effects of soil drying. *Journal of Experimental Botany*, *36*(1), 39–48. https://doi.org/10.1093/jxb/36.1.39

Bonan, G. B., Lawrence, P. J., Oleson, K. W., Levis, S., Jung, M., Reichstein, M., et al. (2011). Improving canopy processes in the Community Land Model version 4 (CLM4) using global flux fields empirically inferred from FLUXNET data. *Journal of Geophysical Research*, *116*, G02014. https://doi.org/10.1029/2010JG001593

Boone, A., Decharme, B., Guichard, F., De Rosnay, P., Balsamo, G., Beljaars, A., et al. (2009). The AMMA Land Surface Model Intercomparison Project (ALMIP). *Bulletin of the American Meteorological Society*, *90*(12), 1865–1880. https://doi.org/10.1175/2009BAMS2786.1

Clapp, R. B., & Hornberger, G. M. (1978). Empirical equations for some soil hydraulic properties. *Water Resources Research*, *14*(4), 601–604. https://doi.org/10.1029/WR014i004p00601

Collatz, G. J., Ball, J. T., Grivet, C., & Berry, J. A. (1991). Physiological and environmental regulation of stomatal conductance, photosynthesis and transpiration: A model that includes a laminar boundary layer. *Agricultural and Forest Meteorology*, *54*(2-4), 107–136. https://doi.org/10.1016/0168-1923(91)90002-8

Collatz, G. J., Ribas-Carbo, M., & Berry, J. (1992). Coupled photosynthesis-stomatal conductance model for leaves of C_4 plants. *Functional Plant Biology*, *19*(5), 519–538. https://doi.org/10.1071/PP9920519

Dorman, J., & Sellers, P. J. (1989). A global climatology of albedo, roughness length and stomatal resistance for atmospheric general circulation models as represented by the simple biosphere model (SiB). *Journal of Applied Meteorology*, *28*(9), 833–855. https://doi.org/10.1175/1520-0450(1989)028%3C0833:AGCOAR%3E2.0.CO;2

Fisher, J. B., Huntzinger, D. N., Schwalm, C. R., & Sitch, S. (2014). Modeling the terrestrial biosphere. *Annual Review of Environment and Resources*, *39*(1), 91–123. https://doi.org/10.1146/annurev-environ-012913-093456

Flexas, J., Escalona, J. M., Evain, S., Gulías, J., Moya, I., Osmond, C. B., & Medrano, H. (2002). Steady-state chlorophyll fluorescence (Fs) measurements as a tool to follow variations of net CO_2 assimilation and stomatal conductance during water-stress in C_3 plants. *Physiologia Plantarum*, *114*(2), 231–240. https://doi.org/10.1034/j.1399-3054.2002.1140209.x

Ford, T., Harris, E., & Quiring, S. (2014). Estimating root zone soil moisture using near-surface observations from SMOS. *Hydrology and Earth System Sciences*, *18*(1), 139–154. https://doi.org/10.5194/hess-18-139-2014

Frankenberg, C., Butz, A., & Toon, G. (2011). Disentangling chlorophyll fluorescence from atmospheric scattering effects in O_2 A-band spectra of reflected sun-light. *Geophysical Research Letters*, *38*, L03801. https://doi.org/10.1029/2010GL045896

Frankenberg, C., Fisher, J. B., Worden, J., Badgley, G., Saatchi, S. S., Lee, J. E., et al. (2011). New global observations of the terrestrial carbon cycle from GOSAT: Patterns of plant fluorescence with gross primary productivity. *Geophysical Research Letters*, *38*, L17706. https://doi.org/10.1029/2011GL048738

Frankenberg, C., O'Dell, C., Berry, J., Guanter, L., Joiner, J., Köhler, P., et al. (2014). Prospects for chlorophyll fluorescence remote sensing from the Orbiting Carbon Observatory-2. *Remote Sensing of Environment*, *147*, 1–12. https://doi.org/10.1016/j.rse.2014.02.007

Friedlingstein, P., Cox, P., Betts, R., Bopp, L., Von Bloh, W., Brovkin, V., et al. (2006). Climate-carbon cycle feedback analysis: Results from the C4MIP model intercomparison. *Journal of Climate*, *19*(14), 3337–3353. https://doi.org/10.1175/JCLI3800.1

Guanter, L., Aben, I., Tol, P., Krijger, J., Hollstein, A., Köhler, P., et al. (2015). Potential of the TROPOspheric Monitoring Instrument (TROPOMI) onboard the Sentinel-5 precursor for the monitoring of terrestrial chlorophyll fluorescence. *Atmospheric Measurement Techniques*, *8*(3), 1337–1352. https://doi.org/10.5194/amt-8-1337-2015

Guanter, L., Alonso, L., Gómez-Chova, L., Amorós-López, J., Vila, J., & Moreno, J. (2007). Estimation of solar-induced vegetation fluorescence from space measurements. *Geophysical Research Letters*, *34*, L08401. https://doi.org/10.1029/2007GL029289

Guanter, L., Zhang, Y., Jung, M., Joiner, J., Voigt, M., Berry, J. A., et al. (2014). Global and time-resolved monitoring of crop photosynthesis with chlorophyll fluorescence. *Proceedings of the National Academy of Sciences of the United States of America*, *111*(14), E1327–E1333. https://doi.org/10.1073/pnas.1320008111

Hari, P., & Makela, A. (2003). Annual pattern of photosynthesis in Scots pine in the boreal zone. *Tree Physiology*, *23*(3), 145–155. https://doi.org/10.1093/treephys/23.3.145

Joiner, J., Guanter, L., Lindstrot, R., Voigt, M., Vasilkov, A. P., Middleton, E. M., et al. (2013). Global monitoring of terrestrial chlorophyll fluorescence from moderate spectral resolution near-infrared satellite measurements: Methodology, simulations, and application to GOME-2. *Atmospheric Measurement Techniques*, *6*(10), 2803–2823. https://doi.org/10.5194/amt-6-2803-2013

Joiner, J., Yoshida, Y., Vasilkov, A., & Middleton, E. (2011). First observations of global and seasonal terrestrial chlorophyll fluorescence from space. *Biogeosciences*, *8*(3), 637–651. https://doi.org/10.5194/bg-8-637-2011

Kahan, D. S., Xue, Y., & Allen, S. J. (2006). The impact of vegetation and soil parameters in simulations of surface energy and water balance in the semi-arid sahel: A case study using SEBEX and HAPEX-Sahel data. *Journal of Hydrology*, *320*(1-2), 238–259. https://doi.org/10.1016/j.jhydrol.2005.07.011

Kang, H.-S., Xue, Y., & Collatz, G. J. (2007). Impact assessment of satellite-derived leaf area index datasets using a general circulation model. *Journal of Climate*, *20*(6), 993–1015. https://doi.org/10.1175/JCLI4054.1

Kerr, Y. H., Al-Yaari, A., Rodriguez-Fernandez, N., Parrens, M., Molero, B., Leroux, D., et al. (2016). Overview of SMOS performance in terms of global soil moisture monitoring after six years in operation. *Remote Sensing of Environment*, *180*, 40–63. https://doi.org/10.1016/j.rse.2016.02.042

Kerr, Y. H., Waldteufel, P., Wigneron, J. P., Delwart, S., Cabot, F., Boutin, J., et al. (2010). The SMOS mission: New tool for monitoring key elements of the global water cycle. *Proceedings of the IEEE*, *98*(5), 666–687. https://doi.org/10.1109/JPROC.2010.2043032

Kerr, Y. H., Waldteufel, P., Wigneron, J. P., Martinuzzi, J., Font, J., & Berger, M. (2001). Soil moisture retrieval from space: The Soil Moisture and Ocean Salinity (SMOS) mission. *IEEE Transactions on Geoscience and Remote Sensing*, *39*(8), 1729–1735. https://doi.org/10.1109/36.942551

Lee, J. E., Berry, J. A., Tol, C., Yang, X., Guanter, L., Damm, A., et al. (2015). Simulations of chlorophyll fluorescence incorporated into the Community Land Model version 4. *Global Change Biology*, *21*(9), 3469–3477. https://doi.org/10.1111/gcb.12948

Lee, J. E., Frankenberg, C., van der Tol, C., Berry, J. A., Guanter, L., Boyce, C. K., et al. (2013). Forest productivity and water stress in Amazonia: Observations from GOSAT chlorophyll fluorescence. *Proceedings of the Royal Society B: Biological Sciences*, *280*(1761), 20130171. https://doi.org/10.1098/rspb.2013.0171

Li, W., Guo, W., Xue, Y., Fu, C., & Qiu, B. (2016). Sensitivity of a regional climate model to land surface parameterization schemes for East Asian summer monsoon simulation. *Climate Dynamics*, *47*(7-8), 2293–2308. https://doi.org/10.1007/s00382-015-2964-8

Lichtenthaler, H. K., & Rinderle, U. (1988). The role of chlorophyll fluorescence in the detection of stress conditions in plants. *Critical Reviews in Analytical Chemistry*, *19*, S29–S85. https://doi.org/10.1080/15476510.1988.10401466

Lokupitiya, E., Denning, A., Schaefer, K., Ricciuto, D., Anderson, R., Arain, M., et al. (2016). Carbon and energy fluxes in cropland ecosystems: A model-data comparison. *Biogeochemistry*, *129*(1-2), 53–76. https://doi.org/10.1007/s10533-016-0219-3

Madani, N., Kimball, J. S., Affleck, D. L., Kattge, J., Graham, J., Bodegom, P. M., et al. (2014). Improving ecosystem productivity modeling through spatially explicit estimation of optimal light use efficiency. *Journal of Geophysical Research: Biogeosciences*, *119*, 1755–1769. https://doi.org/10.1002/2014JG002709

Meroni, M., Rossini, M., Picchi, V., Panigada, C., Cogliati, S., Nali, C., & Colombo, R. (2008). Assessing steady-state fluorescence and PRI from hyperspectral proximal sensing as early indicators of plant stress: The case of ozone exposure. *Sensors*, *8*(12), 1740–1754. https://doi.org/10.3390/s8031740

Niu, G. Y., Yang, Z. L., Mitchell, K. E., Chen, F., Ek, M. B., Barlage, M., et al. (2011). The community Noah land surface model with multiparameterization options (Noah-MP): 1. Model description and evaluation with local-scale measurements. *Journal of Geophysical Research*, *116*, D12109. https://doi.org/10.1029/2010JD015139

Qiu, B., Guo, W., Xue, Y., & Dai, Q. (2016). Implementation and evaluation of a generalized radiative transfer scheme within canopy in the soil-vegetation-atmosphere transfer (SVAT) model. *Journal of Geophysical Research: Atmospheres*, *121*, 12,145–12,163. https://doi.org/10.1002/2016JD025328

Rascher, U., Alonso, L., Burkart, A., Cilia, C., Cogliati, S., Colombo, R., et al. (2015). Sun-induced fluorescence—A new probe of photosynthesis: First maps from the imaging spectrometer HyPlant. *Global Change Biology*, *21*(12), 4673–4684. https://doi.org/10.1111/gcb.13017

Richardson, A. D., Anderson, R. S., Arain, M. A., Barr, A. G., Bohrer, G., Chen, G., et al. (2012). Terrestrial biosphere models need better representation of vegetation phenology: Results from the North American Carbon Program Site Synthesis. *Global Change Biology*, *18*(2), 566–584. https://doi.org/10.1111/j.1365-2486.2011.02562.x

Rienecker, M. M., Suarez, M. J., Gelaro, R., Todling, R., Bacmeister, J., Liu, E., et al. (2011). MERRA: NASA's modern-era retrospective analysis for research and applications. *Journal of Climate*, *24*(14), 3624–3648. https://doi.org/10.1175/JCLI-D-11-00015.1

Running, S. W., Nemani, R. R., Heinsch, F. A., Zhao, M., Reeves, M., & Hashimoto, H. (2004). A continuous satellite-derived measure of global terrestrial primary production. *Bioscience*, *54*(6), 547–560. https://doi.org/10.1641/0006-3568(2004)054%5B0547:ACSMOG%5D2.0.CO;2

Rutter, N., Essery, R., Pomeroy, J., Altimir, N., Andreadis, K., Baker, I., et al. (2009). Evaluation of forest snow processes models (SnowMIP2). *Journal of Geophysical Research*, *114*, D06111. https://doi.org/10.1029/2008JD011063

Saltelli, A., Annoni, P., Azzini, I., Campolongo, F., Ratto, M., & Tarantola, S. (2010). Variance based sensitivity analysis of model output. Design and estimator for the total sensitivity index. *Computer Physics Communications*, *181*(2), 259–270. https://doi.org/10.1016/j.cpc.2009.09.018

Saltelli, A., Tarantola, S., & Chan, K. S. (1999). A quantitative model-independent method for global sensitivity analysis of model output. *Technometrics*, *41*(1), 39–56. https://doi.org/10.2307/1270993

Scholze, M., Kaminski, T., Knorr, W., Blessing, S., Vossbeck, M., Grant, J., & Scipal, K. (2016). Simultaneous assimilation of SMOS soil moisture and atmospheric CO_2 in-situ observations to constrain the global terrestrial carbon cycle. *Remote Sensing of Environment*, *180*, 334–345. https://doi.org/10.1016/j.rse.2016.02.058

Sellers, P. J., Randall, D. A., Collatz, G. J., Berry, J. A., Field, C. B., Dazlich, D. A., et al. (1996). A revised land surface parameterization (SiB2) for atmospheric GCMS. Part I: Model formulation. *Journal of Climate*, *9*(4), 676–705. https://doi.org/10.1175/1520-0442(1996)009%3C0676:ARLSPF%3E2.0.CO;2

Sheffield, J., Goteti, G., & Wood, E. F. (2006). Development of a 50-year high-resolution global dataset of meteorological forcings for land surface modeling. *Journal of Climate*, *19*(13), 3088–3111. https://doi.org/10.1175/JCLI3790.1

Sun, Y., Frankenberg, C., Wood, J. D., Schimel, D. S., Jung, M., Guanter, L., et al. (2017). OCO-2 advances photosynthesis observation from space via solar-induced chlorophyll fluorescence. *Science*, *358* (6360), eaam5747. https://doi.org/10.1126/science.aam5747

Sun, Y., Fu, R., Dickinson, R., Joiner, J., Frankenberg, C., Gu, L., et al. (2015). Drought onset mechanisms revealed by satellite solar-induced chlorophyll fluorescence: Insights from two contrasting extreme events. *Journal of Geophysical Research: Biogeosciences*, *120*, 2427–2440. https://doi.org/10.1002/2015JG003150

Turner, D. P., Urbanski, S., Bremer, D., Wofsy, S. C., Meyers, T., Gower, S. T., & Gregory, M. (2003). A cross-biome comparison of daily light use efficiency for gross primary production. *Global Change Biology*, *9*(3), 383–395. https://doi.org/10.1046/j.1365-2486.2003.00573.x

van der Tol, C., Berry, J., Campbell, P., & Rascher, U. (2014). Models of fluorescence and photosynthesis for interpreting measurements of solar-induced chlorophyll fluorescence. *Journal of Geophysical Research: Biogeosciences*, *119*, 2312–2327. https://doi.org/10.1002/2014JG002713

van der Tol, C., Verhoef, W., Timmermans, J., Verhoef, A., & Su, Z. (2009). An integrated model of soil-canopy spectral radiances, photosynthesis, fluorescence, temperature and energy balance. *Biogeosciences*, *6*(12), 3109–3129. https://doi.org/10.5194/bg-6-3109-2009

Verrelst, J., Pablo Rivera, J., Tol, C.v.d., Magnani, F., Mohammed, G., & Moreno, J. (2015). Global sensitivity analysis of the scope model: What drives simulated canopy-leaving Sun-induced fluorescence? *Remote Sensing of Environment*, *166*, 8–21. https://doi.org/10.1016/j.rse.2015.06.002

Wang, W., Dungan, J., Hashimoto, H., Michaelis, A. R., Milesi, C., Ichii, K., & Nemani, R. R. (2011). Diagnosing and assessing uncertainties of terrestrial ecosystem models in a multimodel ensemble experiment: 1. Primary production. *Global Change Biology*, *17*(3), 1350–1366. https://doi.org/10.1111/j.1365-2486.2010.02309.x

Xue, Y., Fennessy, M. J., & Sellers, P. J. (1996). Impact of vegetation properties on U.S. summer weather prediction. *Journal of Geophysical Research*, *101*, 7419–7430. https://doi.org/10.1029/95JD02169

Xue, Y., Janjic, Z., Dudhia, J., Vasic, R., & De Sales, F. (2014). A review on regional dynamical downscaling in intraseasonal to seasonal simulation/prediction and major factors that affect downscaling ability. *Atmospheric Research*, *147-148*, 68–85. https://doi.org/10.1016/j.atmosres.2014.05.001

Xue, Y., Sellers, P., Kinter, J. L., & Shukla, J. (1991). A simplified biosphere model for global climate studies. *Journal of Climate*, *4*(3), 345–364. https://doi.org/10.1175/1520-0442(1991)004%3C0345:ASBMFG%3E2.0.CO;2

Xue, Y., Sellers, P. J., Zeng, F. J., & Schlosser, C. A. (1997). Comments on "Use of midlatitude soil moisture and meteorological observations to validate soil moisture simulations with biosphere and bucket models". *Journal of Climate*, *10*(2), 374–376. https://doi.org/10.1175/1520-0442(1997)010%3C0374:COUOMS%3E2.0.CO;2

Xue, Y., Zeng, F. J., & Schlosser, C. A. (1996). SSiB and its sensitivity to soil properties—A case study using HAPEX-Mobilhy data. *Global and Planetary Change*, *13*(1-4), 183–194. https://doi.org/10.1016/0921-8181(95)00045-3

Yang, X., Tang, J., Mustard, J. F., Lee, J. E., Rossini, M., Joiner, J., et al. (2015). Solar-induced chlorophyll fluorescence that correlates with canopy photosynthesis on diurnal and seasonal scales in a temperate deciduous forest. *Geophysical Research Letters*, *42*, 2977–2987. https://doi.org/10.1002/2015GL063201

Yoshida, Y., Joiner, J., Tucker, C., Berry, J., Lee, J.-E., Walker, G., et al. (2015). The 2010 Russian drought impact on satellite measurements of solar-induced chlorophyll fluorescence: Insights from modeling and comparisons with parameters derived from satellite reflectances. *Remote Sensing of Environment*, *166*, 163–177. https://doi.org/10.1016/j.rse.2015.06.008

Zhan, X., Xue, Y., & Collatz, G. J. (2003). An analytical approach for estimating CO_2 and heat fluxes over the Amazonian region. *Ecological Modelling*, *162*(1-2), 97–117. https://doi.org/10.1016/S0304-3800(02)00405-2

Zhang, Z., Xue, Y., MacDonald, G., Cox, P. M., & Collatz, G. J. (2015). Investigation of North American vegetation variability under recent climate: A study using the SSiB4/TRIFFID biophysical/dynamic vegetation model. *Journal of Geophysical Research: Atmospheres*, *120*, 1300–1321. https://doi.org/10.1002/2014JD021963